ELSEVIER

Applied Catalysis B: Environmental 31 (2001) 241–249

APPLIED CATALYSIS B: ENVIRONMENTAL

www.elsevier.com/locate/apcatb

Photodegradation of aromatic pollutants in water over TiO_2 supported on molecular sieves

Yu-Hsiang Hsien, Chi-Fu Chang, Yu-Huang Chen, Soofin Cheng*

Department of Chemistry, National Taiwan University, Taipei 106, Taiwan, ROC

Received 28 June 2000; received in revised form 22 November 2000; accepted 22 November 2000

Abstract

TiO_2 was supported on porous materials, including NaY and Na-mordenite zeolites, as well as mesoporous MCM-41 molecular sieve by using impregnation method with organic solvents. The products were characterized with powder XRD, BET surface area measurement, TEM, IR, Raman and UV–VIS spectroscopies. The supported TiO_2 was crystallized in anatase structure and the intensity of its X-ray diffraction peaks increased with TiO_2 loading. In contrast, the total surface area of the supported catalyst decreased with TiO_2 loading. A blue shift of the absorption edge in the UV–VIS spectra was observed when TiO_2 particle size decreased, a phenomenon corresponding to the particle size quantization effect. For photodegradation of aromatic pollutants in water, the activity was found strongly influenced by the chemical nature of the pollutant and the surface property of the support. For volatile pollutants such as benzene and chlorobenzenes, molecular sieve supports facilitated the photodegradation reaction by providing high surface area for adsorption. Moreover, there is an optimal loading of TiO_2 to achieve the best photocatalytic activity on various supports. The supports in contrast did not show positive contribution in degradation of hydrophilic pollutants such as phenol.

Keywords: TiO_2; Photodegradation; Aromatic pollutants; Zeolites

1. Introduction

The photocatalytic degradation of organic pollutants in waste water has attracted a great attention in the past two decades [1,2]. Due to its stability and non-toxicity, TiO_2 has been the most investigated as the photocatalyst. The band gap of this "semiconductor" material is ca. 3.2 eV, which corresponds to radiation of wavelength around 380 nm [3]. Therefore, an UV light with wavelength shorter than 380 nm is needed to excite the electrons in valence band to conduction band. The electron–hole pairs thus generated serve as the oxidizing and reducing agents. In photodegradation of pollutants in water, $^{\bullet}OH$ radicals formed either through the interaction of water molecule with the hole or through the interaction of O_2 with the hot electron are the key active species [4,5]. The efficiency of TiO_2 was reported to be influenced by many factors, such as crystalline structure [6–8], particle size [7,9–11], and preparation methods [12,13]. In the past few years, some efforts have been put in increasing the TiO_2 surface area by dispersing nano-particles of TiO_2 on high surface area materials. The support been used included silica gels, active carbon, zeolites and clays [9,14–17]. Some of these studies have also included an effort to increase the adsorption of organic substrates on the catalyst surface for improving the efficiency of catalytic activity [17–19]. In the present study, TiO_2 was supported on

* Corresponding author. Tel.: +886-2-23638017; fax: +886-2-23636359.

0926-3373/01/$ – see front matter
PII: S0926-3373(00)00283-6

three porous materials, namely NaY, Na-mordenite, and MCM-41. The first two were microporous zeolites with pore diameters around 0.76 nm, while the latter was meso-porous molecular sieve with a pore diameter of 2.6 nm. The aromatic pollutants under investigation were benzene, chlorobenzene, 1,2-dichlorobenzene and phenol. The hydrophilicity of the pollutants as well as that of the supports was found to play important role in the photodegradation activities.

2. Experimental methods

2.1. Catalyst preparation

Reagent grade chemicals were used as purchased without further purification. TiO_2 of anatase form was purchased from Merck. That of rutile form was from Jassen. Degussa P-25 TiO_2, which contains anatase/rutile (ca. 3/1) mixed phases was also used for comparison in photocatalytic studies. The supported TiO_2 catalysts were prepared by impregnation method. NaY and Na-mordenite zeolites were obtained from Tosoh Corporation, Japan, as Asia reference catalysts numbers 22 and 26, respectively. MCM-41 was prepared by delayed neutralization method according to the procedures mentioned in [20]. The as-synthesized MCM-41 without calcination was used in preparation of the supported catalysts. The Ti-source $Ti(OEt)_4$ was added to the support powders suspended in the solvent composed of hexane/heptane with volumetric ratio of 1/1, and the mixture was stirred for 1 h in air to hydrolyze $Ti(OEt)_4$. Then the solvent was removed by rotary evaporation. The resultant solid was dried at 100°C and calcined at 550–560°C for 6 h.

2.2. Characterization of the catalysts

The materials were examined with powder XRD, BET surface area measurement, TEM, IR, Raman and UV–VIS spectroscopies. The powder XRD patterns were collected on a Scintag X1 X-ray diffractometer using Cu Kα radiation. The patterns were taken over the 2θ range of 1.5–70°. The BET surface area and pore diameter of the catalysts were determined by physical adsorption of nitrogen at −196°C in a Micromeritics ASAP 2010 analyzer. UV–VIS spectra of the powder samples were measured using Shimadzu UV-2101PC spectrophotometer. The TEM photographs were taken with a Hitachi H-7100 electron microscopy. The IR/Raman spectra were measured with a Bomem MB155 FT-IR/Roman spectrometer.

2.3. Photocatalytic activity measurements

The photodegradation experiments were carried out in a quartz tubular reactor placed inside a Rayoney photochemical chamber (Model PRP-100) with 300 nm UV irradiation source. The catalyst in powder form based on the same metal equivalence as 0.01 g TiO_2, was suspended in 50 ml aqueous solution of 0.5 mM organic pollutants. The organic pollutants under investigation included benzene, monochlorobenzene (MCB), 1,2-dichlorobenzene (DCB), and phenol. The reactor was kept at 20 ± 2°C with cooling water circulation during the experiments. A flow of oxygen (2 ml/min) bubbling into the reactor, served as the oxidant. The outlet gases were directed through a two-stage bubbling trap containing saturated $Ba(OH)_2$ solution, and the CO_2 yield was determined based on the weight of $BaCO_3$ precipitated. Gas products were analyzed off-line during the reaction course, and liquid products retained in aqueous solution after 6 h radiation were separated with a Hewlett-Packard 5890 GC using a Rtx-5 capillary column of 60 m length and detected by a FID detector.

3. Results and discussion

3.1. Catalyst characterization

Figs. 1–3 are the XRD patterns of TiO_2 supported on various molecular sieves with different TiO_2 loadings. The crystalline structures of the molecular sieves were well retained. Over NaY and Na-mordenite supports, the peaks corresponding to anatase TiO_2 appeared at $2\theta = 25.4$, 37.9, 48.2, 54.0, 55.2 and 62.8° and their intensity grew with TiO_2 loading. However, over MCM-41, these peaks appeared only as small bumps even with 30% TiO_2 loading. The FT-Raman spectra of the supported catalysts confirmed that the TiO_2 formed on all three supports was in anatase structure. Fig. 4 shows that the characteristic Raman peaks for anatase appear at 399, 516 and 640 cm^{-1}. Again, the peaks observed on TiO_2 supported on MCM-41

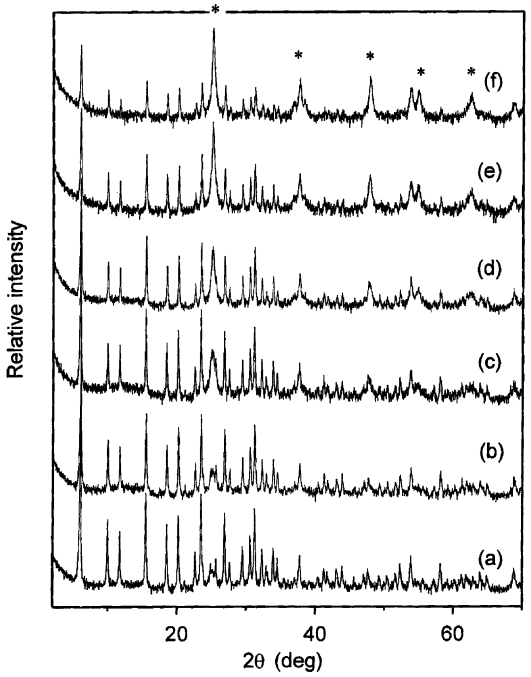

Fig. 1. XRD patterns of TiO_2 supported on NaY zeolite with TiO_2 loading of (a) 5%; (b) 10%; (c) 20%; (d) 30%; (e) 45%; and (f) 60% (* labels the diffraction peaks of anatase TiO_2).

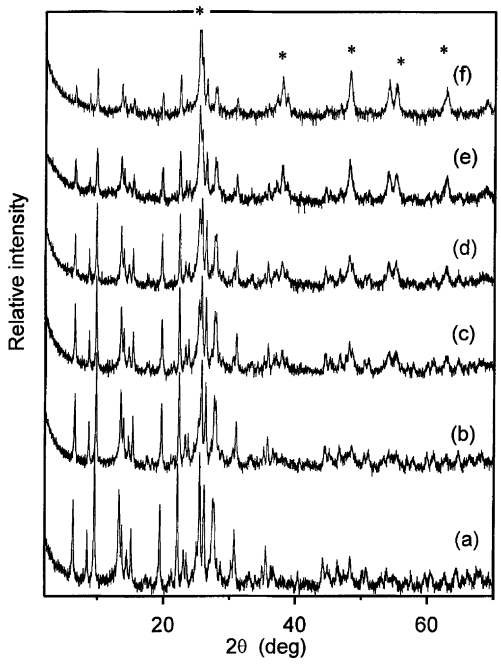

Fig. 2. XRD patterns of TiO_2 supported on Na-mordenite with TiO_2 loading of (a) 5%; (b) 10%; (c) 20%; (d) 30%; (e) 45%; and (f) 60% (* labels the diffraction peaks of anatase TiO_2).

are much weaker than that supported on NaY and Na-mordenite. These results imply that the TiO_2 particles formed on MCM-41 were much smaller than those on NaY and Na-mordenite. However, over the same support, the size of TiO_2 particle increased with TiO_2 loading.

Fig. 5 shows the TEM photographs of NaY and MCM-41 before and after they were loaded with 30% TiO_2. The pristine NaY granules are in the diameter of ca. 200–300 nm and have smooth external surfaces. On the NaY supported TiO_2 sample, small crystallites of ca. 10–20 nm diameter can be clearly seen aggregated on the external surfaces of NaY granules. For MCM-41, the channels and holes in hexagonal arrangement are seen on the pristine MCM-41. On the TiO_2 loaded sample, small dark spots seem to spread all over the particles of MCM-41 and no aggregation of crystallites on the external surfaces is seen. These results indicate that TiO_2 supported on zeolites probably cannot get into the micropores and it forms small crystallites aggregated on the external surfaces of the zeolite granules. On the other hand, TiO_2 supported on MCM-41 may disperse inside the mesopores. In addition, TiO_2 in the latter case forms smaller particles than that supported on microporous zeolites because of the high surface area of MCM-41.

Table 1 shows the BET surface areas of the catalysts as well as the particle diameter estimated by Scherrer's equation and the bandgap of the TiO_2 particles. The bandgap energies of the catalysts were determined based on the absorption threshold of their UV–VIS spectra. The total surface area of the supported catalysts was found to decrease with TiO_2 loading. It implies that some of the pores of the molecular sieves were blocked by the TiO_2 particles. The benefit of using mesoporous molecular sieve is shown by that relative large surface area of ca. 700 m^2/g was still retained with 30% TiO_2 loading, while at the same loading level, 530 and 250 m^2/g were obtained over NaY and Na-mordenite, respectively.

The TiO_2 particle diameter was estimated with Scherrer's equation using the line-width at half-maximum of the X-ray diffraction peaks at $2\theta = 25.4$ and 27.5° for anatase and rutile, respectively. The

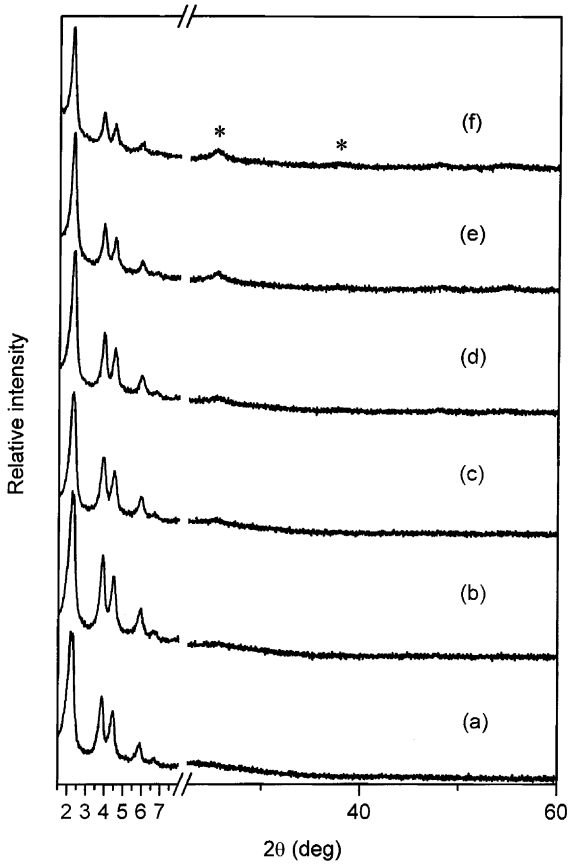

Fig. 3. XRD patterns of TiO_2 supported on MCM-41 with TiO_2 loading of (a) 0%; (b) 2%; (c) 5%; (d) 10%; (e) 20%; and (f) 30% (* labels the diffraction peaks of anatase TiO_2).

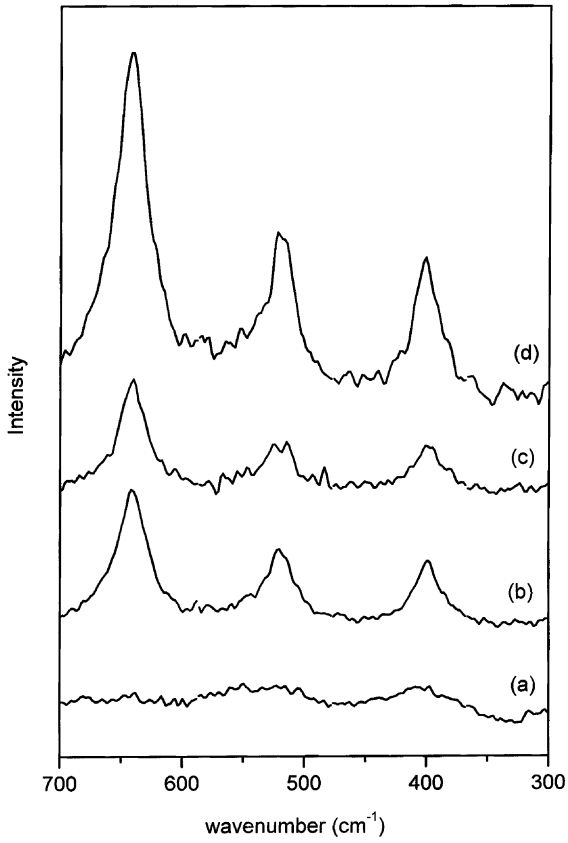

Fig. 4. FT-Raman spectra of supported TiO_2: (a) 10% on MCM-41; (b) 10% on mordenite; (c) 10% on NaY; (d) 30% on MCM-41; (e) 30% on NaY; (f) 30% on mordenite; and (g) commercial anatase TiO_2.

particle sizes estimated by Scherrer's equation are generally larger than that observed on TEM. That is due to that the detection limit for XRD is around 2 nm. It was also found that the particle diameters were too small to estimate for samples with TiO_2 loadings less than 20%. Nevertheless, the values show that the size of TiO_2 particles increases with TiO_2 loading. Over different supports, the variation of TiO_2 particle size was in the reverse order of the surface area. In other words, the TiO_2 particle diameter decreases in the order of Na-mordenite > NaY > MCM-41.

Over the same support, the bandgap energy decreases with the increase in TiO_2 loading and the TiO_2 diameter. That is in consistence with "particle size quantization effect" [22]. It is also seen that commercial rutile has the smallest value in bandgap, which is attributed to its relatively dense-packing crystalline structure in comparison to anatase structure [21]. The very low surface area, which in turn means very large particle size, of the rutile sample may also have some contribution to the very small band edge. Degussa P-25 which contains mixed phases of anatase and rutile has the highest surface area among the commercial TiO_2, and the bandgap is close to that of anatase.

3.2. Photocatalytic activity

Table 2 compares the photocatalytic activities of TiO_2 supported on various molecular sieves with those over pure TiO_2. The degradation efficiency presented as CO_2 yield was strongly influenced by the volatility and nucleophilicity of the pollutants. For the volatile

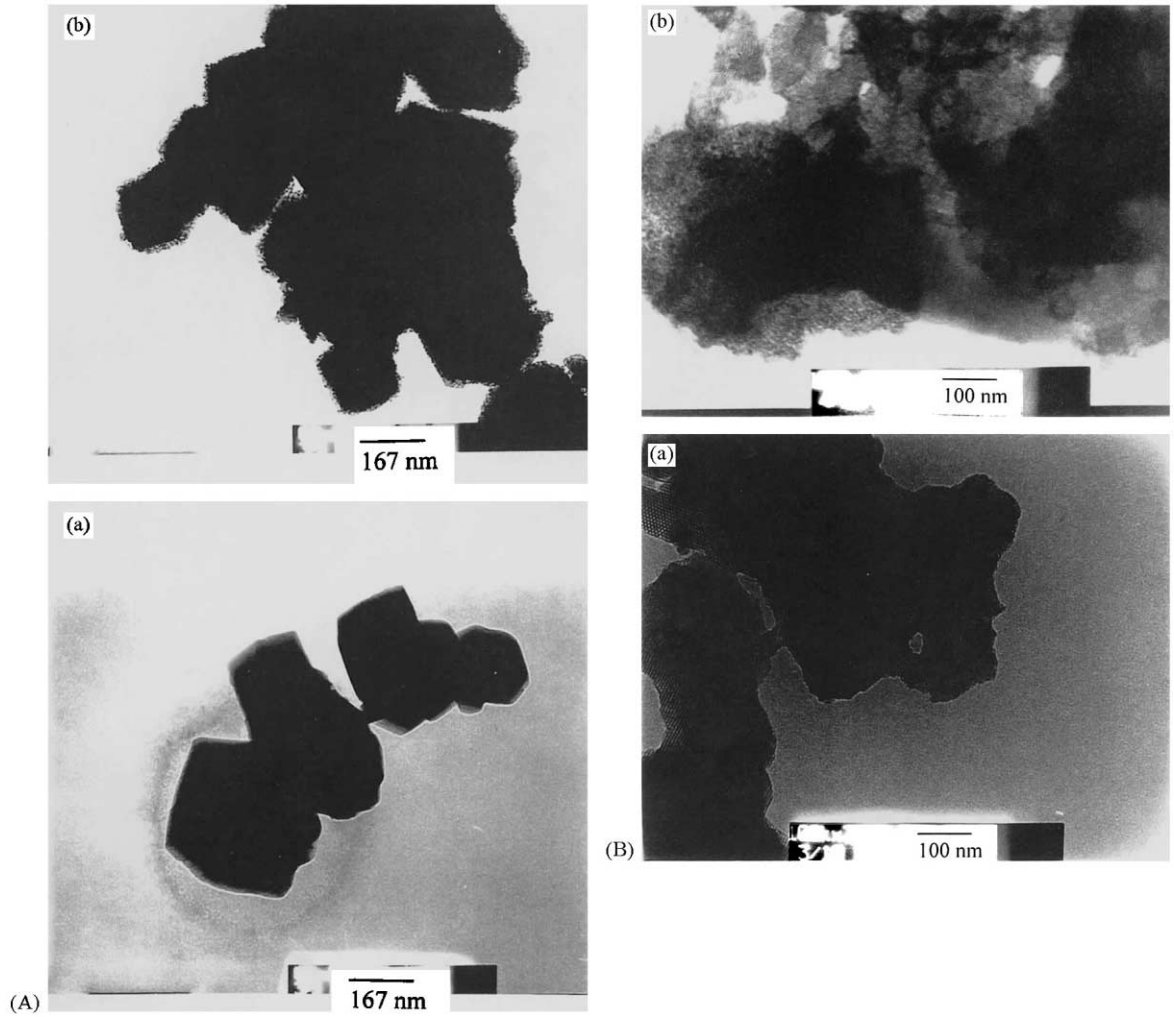

Fig. 5. TEM photographs of (A) NaY; (B) MCM-41 before (a) and after (b) loaded with 30% TiO_2.

pollutants such as benzene and monochlorobenzene, the CO_2 yields were lower and a portion of these pollutants was dissipated into the gas flow. On the other hand, phenol which is a better nucleophile than other aromatic pollutants reacts more easily with $^{\bullet}OH$ radicals and has the highest degradation efficiency.

Over the commercially available TiO_2 catalysts, Degussa P-25 was the one most efficient in mineralization of the aromatic pollutants. On the other hand, anatase gave much higher catalytic activities than rutile. That is consistent with what reported in the literature. The explanations are still debatable, which includes electron–hole recombination rate [8], number of surface hydroxyl group [12], and surface defects [23]. Judging from that P-25 contains anatase/rutile mixed phases and relatively high surface area, the high activities of P-25 is likely attributed to the large quantity of structural and surface defects in this commercial TiO_2 product. For the purpose of examining the effect of the supports, the catalytic activity of P-25 would not be emphasized hereafter since the supported catalysts had TiO_2 in pure anatase phase.

Over the supported TiO_2 catalysts, the catalytic activity was found to vary with the hydrophilicity of

Table 1
BET surface area, particle size, and bandgap values of commercial and supported TiO_2

Catalyst (TiO_2 loading)	Surface area (m^2/g)	TiO_2 particle diameter (nm)[a]	Band gap (eV)
NaY support			
0%	851	–	–
5%	716	–	3.25
10%	658	–	3.23
20%	596	20.7	3.19
30%	532	21.2	3.17
45%	400	22.0	3.15
60%	276	27.3	3.13
Na-mordenite support			
0%	383	–	–
5%	364	–	3.26
10%	348	–	3.23
20%	324	–	3.20
30%	253	30.9	3.19
45%	231	39.8	3.15
60%	148	52.1	3.11
MCM-41 support			
0%	1009	–	–
2%	997	–	3.23
5%	954	–	3.22
10%	891	–	3.19
20%	811	4.5	3.18
30%	701	5.6	3.15
Commercial TiO_2			
Anatase	34	62.7	3.09
Rutile	6	64.7	2.86
P-25	54	–	3.04

[a] Determined by Scherrer's equation with the (1 0 1) and (1 1 0) peaks on XRD patterns for anatase and rutile, respectively.

the pollutants. For the decomposition of hydrophobic compounds such as benzene, MCB, and DCB, some of the molecular sieve-supported TiO_2 catalysts gave better activities than the commercial anatase TiO_2 or even P-25. Furthermore, there was an optimal TiO_2 loading and this value varied with the support. The optimal loading was 30% on NaY, 20–30% on Na-mordenite and 10% on MCM-41. In contrast, for degradation of hydrophilic pollutant phenol, most of the supported TiO_2 catalysts were not as active as the commercial TiO_2, except that the 10%TiO_2/MCM-41 has similar activity as commercial anatase.

In comparison of the amount of volatile pollutants dissipated into the gas phase, molecular sieves seem to be effective in adsorption of the volatile pollutants. They probably also facilitated the photodegradation reaction through transferring the organic adsorbates to the TiO_2 crystallites nearby and resulted in higher mineralization efficiency. Table 2 shows that the amounts of benzene and MCB dissipated into the gas phase are much lower over molecular sieve-supported TiO_2 catalysts. In general, the amount of dissipated pollutants decreases with the increase in total surface area. However, MCM-41 which has highest surface area does not give better photodegradation activity toward benzene than NaY. It is attributed to that large amount of OH groups presented on MCM-41 surface probably makes it rather hydrophilic. As a result, the surface has less tendency to adsorb benzene which is a non-polar and hydrophobic molecule. In contrast, the surface hydrophilicity of MCM-41 facilitates the adsorption of polar or hydrophilic pollutants. Indeed, MCM-41 supported TiO_2 catalysts were the most active among the three molecular

Table 2
The results of photodegradation of various aromatic pollutants in water

Catalyst (TiO_2 loading)	Benzene		MCB		DCB	Phenol
	CO_2 yield (%)	Dis. (%)[a]	CO_2 yield (%)	Dis. (%)	CO_2 yield (%)	CO_2 yield (%)
NaY support						
5%	23.7	5.6	27.1	1.0	30.9	43.3
10%	30.8	9.5	33.8	1.2	44.7	49.4
20%	35.8	10.9	37.5	2.1	52.2	53.7
30%	39.4	9.9	46.6	2.4	61.1	69.0
45%	37.2	13.7	40.6	5.8	53.1	62.5
60%	16.9	17.9	32.1	7.5	35.1	46.6
Na-mordenite support						
5%	21.0	17.3	32.4	2.2	34.8	31.8
10%	29.7	15.1	34.7	2.8	44.5	61.5
20%	31.8	9.3	45.2	4.1	57.2	68.9
30%	36.5	8.6	36.2	5.2	53.3	66.2
45%	30.7	18.3	31.0	4.7	45.8	60.1
60%	12.8	22.1	19.9	4.8	42.7	47.3
MCM-41 support						
2%	25.0	7.6	37.8	0.6	43.6	57.4
5%	31.1	5.8	44.3	0.7	51.4	65.9
10%	33.1	5.9	51.4	0.7	69.1	78.3
20%	29.1	8.3	38.9	1.4	60.5	63.5
30%	27.0	16.0	36.8	4.2	41.2	39.9
Commercial TiO_2						
Anatase	25.0	30.2	38.0	5.9	41.9	78.0
Rutile	17.6	26.2	18.0	18.0	11.7	26.9
P-25	36.6	–	–	–	–	∼100

[a] Dis.: dissipation to the gas phase.

Table 3
Adsorption capabilities towards phenol and benzene in aqueous solutions on various TiO_2 catalysts[a]

Catalyst (TiO_2 loading)	Equilibrium adsorbed amount in aqueous solutions			
	Phenol		Benzene	
	10^{-4} mol/g catalyst	10^{-4} mol/g TiO_2	10^{-4} mol/g catalyst	10^{-4} mol/g TiO_2
NaY support	0.22	–	0.17	–
10%	0.35	3.5	0.92	9.2
20%	0.66	3.3	1.35	6.75
30%	0.78	2.6	1.80	6.0
Na-mordenite support	0.34	–	0.20	–
10%	0.17	1.7	0.46	4.6
20%	0.27	1.35	0.94	4.7
30%	0.43	1.43	1.54	5.1
MCM-41 support	0.12	–	0.18	–
20%	1.04	5.2	0.97	4.85
Commercial TiO_2				
Anatase	2.11	2.11	2.95	2.95
Rutile	0.86	0.86	1.70	1.70

[a] Started with 5×10^{-4} M aromatics in water at 20°C.

sieve supports in degradation of MCB, 1,2-DCB and phenol.

Table 3 compares the adsorption capabilities toward phenol and benzene in aqueous solutions on various TiO_2 catalysts. In order to imitate the reaction condition, the catalyst in powder form containing 0.01 g TiO_2 was suspended in 50 ml of 0.5 mM solution of either phenol or benzene. In order to study the adsorption capabilities of the supports themselves, 0.1 g of the molecular sieves was used instead. The mixture was sealed in a plastic bottle and kept shaking at 20°C in dark for 24 h. The equilibrium adsorbed amount of the aromatic adsorbate was determined by analyzing the amount of compound left in the liquid phase using gas chromatograph. A small amount of cyclohexanone of known concentration was added into the separated liquid as internal standard.

The values shown in Table 3 are to some extent controversy to our prediction. Pure TiO_2 of either anatase or rutile phase adsorbed more phenol and benzene than the pristine molecular sieve supports. Besides, the adsorption capacities towards benzene are similar for the three molecular sieve supports, while the microporous NaY and Na-mordenite have higher adsorption capacities towards phenol than MCM-41. These results are attributed to that the adsorption experiments were carried out in very diluted aqueous solutions. Water molecules, which are much more polar than phenol and benzene, should compete with the aromatics for adsorption. In other words, the molecular sieves themselves, especially MCM-41, favor adsorption of water than the aromatic compounds when comparing with TiO_2. A general trend is seen that the adsorption capacities of the aromatic adsorbates increase with the TiO_2 loading on the molecular sieves. In other words, TiO_2 dispersed on the molecular sieve surfaces helps the adsorption of aromatics. However, by converting the basis of adsorption capacity from per gram of catalyst to per gram of TiO_2, it was found that the adsorption capacities improve greatly on the supported TiO_2 except Na-mordenite. Therefore, the adsorption behavior is not simply contributed by TiO_2.

For supported catalysts of the same TiO_2 loading, the adsorption capacity of phenol is directly proportional to the total surface area of the catalyst, while that of benzene is not. Moreover, NaY and Na-mordenite supported TiO_2 adsorbs much more benzene than phenol, while MCM-41 supported TiO_2 adsorbs almost the same or slightly more phenol. Since the TiO_2 on NaY and Na-mordenite forms small crystallites and aggregated on the outer surfaces of the zeolite granules, most of the surface area are likely contributed by the porous structures of zeolites. Although pure anatase TiO_2 also adsorbs more benzene than phenol, the great increase in adsorption capacity of benzene based on per gram of TiO_2 on the zeolite-supported catalysts implies that the surfaces of NaY and Na-mordenite are relatively more hydrophobic. In contrast, the phenol adsorption capacities based on per gram of TiO_2 have slight increases on NaY-supported TiO_2 but decreases on Na-mordenite supported catalysts. Relatively, the phenol adsorption capacity improves significantly on MCM-41 supported TiO_2. These results support our proposal that the photodegradation efficiency of volatile pollutants such as benzene and MCB is enhanced with molecular sieve supports of hydrophobic surfaces due to their assistance in adsorption.

Table 4
The luminescence lifetime of commercial and supported TiO_2

Catalyst	Lifetime (μs)
NaY support	
5%	0.40 ± 0.01
10%	0.41 ± 0.01
20%	0.40 ± 0.01
30%	0.44 ± 0.02
45%	0.42 ± 0.02
60%	0.34 ± 0.02
Na-mordenite support	
5%	0.43 ± 0.01
10%	0.44 ± 0.01
20%	0.48 ± 0.02
30%	0.58 ± 0.01
45%	0.46 ± 0.01
60%	0.39 ± 0.01
MCM-41 support	
2%	0.39 ± 0.01
5%	0.43 ± 0.01
10%	0.46 ± 0.01
20%	0.42 ± 0.02
30%	0.38 ± 0.01
Commercial TiO_2	
Anatase	0.44 ± 0.02
Rutile	0.31 ± 0.01

It is interesting to see that there is an optimal loading of TiO_2 to obtain the best photocatalytic activity on various supports. Similar results were also observed by Zhang et al. [10]. A fast electron–hole recombination on the surface of TiO_2 was proposed for the low activities of smaller TiO_2 particles, while a fast electron–hole recombination in the bulk of TiO_2 was proposed for the low activities of larger TiO_2 particles. In this study, the lifetime of radiation-excited electrons of various TiO_2 catalysts was determined with a time-resolved spectrometer, in which 355 nm light source generated from a Nd-YAG laser was used and detection was set at 450 nm to monitor the luminescence lifetime [11]. Table 4 shows the results of the luminescence lifetime, which in turn is proportional to the lifetime of the excited electrons in the conduction band. The results show that commercial rutile has the shortest luminescence lifetime, implying the fastest electron–hole recombination. The variation of the luminescence lifetime as a function of TiO_2 loading on the specific support was in good agreement with the photocatalytic activity. The catalyst which gave the highest photocatalytic activity has an optimal luminescence lifetime. These results are in consistence with the proposal given by Zhang et al. [10]. As to the effect of different supports, factors other than the lifetime of the excited electrons, such as surface area and hydrophilicity, should play important roles in determining the photocatalytic activity.

Acknowledgements

Financial support from China Petroleum Corporation, Taiwan is gratefully acknowledged. The authors are also thankful to Tosoh Chemicals, Japan for the free samples of NaY and mordenite zeolites provided as Asia reference catalysts.

References

[1] R.W. Mattews, Water Res. 24 (1990) 653.
[2] R.W. Mattews, J. Catal. 113 (1988) 549.
[3] M. Gratzel, in: N. Serpone, E. Pelizzetti (Eds.), Photocatalysis: Fundamentals and Applications, Wiley, New York, 1989, p. 123.
[4] H. Al-Ekabi, N. Sperpone, E. Pelizzetti, C. Minero, Langmuir 5 (1989) 250.
[5] C.S. Turchi, D.F. Ollis, J. Catal. 119 (1989) 4483.
[6] S.I. Nishimoto, B. Ohtani, H. Kajiwara, T. Kagiya, J. Chem. Soc., Faraday Trans. 1 81 (1985) 61.
[7] K. Tanaka, T. Hisanaga, A.P. Rivera, in: D.F. Ollis, H. Al-Ekabi (Eds.), Photocatalytic Purification and Treatment of Water and Air, Elsevier, Amsterdam, 1993, p. 169.
[8] M.A. Fox, M.T. Dulay, Chem. Rev. 95 (1993) 541.
[9] H. Yoneyama, S. Yamanaka, S. Haga, J. Phys. Chem. 83 (1989) 4833.
[10] Z. Zhang, C.C. Wang, R. Zakaria, J. Ying, J. Phys. Chem. B 102 (1998) 10871.
[11] S.-J. Tsai, S. Cheng, Catal. Today 33 (1997) 227.
[12] A. Sclafani, L. Palmisano, M. Schiavello, J. Phys. Chem. 94 (1990) 829.
[13] N. Serpone, D. Lawless, R. Khairutdinov, J. Phys. Chem. 99 (1995) 16655.
[14] S. Sato, Langmuir 4 (1988) 1156.
[15] S. Sampath, H. Uchida, H. Yoneyama, J. Catal. 149 (1994) 148.
[16] X. Liu, K.K. Iu, J.K. Thomas, J. Chem. Soc., Faraday Trans. 89 (1993) 1816.
[17] C. Anderson, A.J. Bard, J. Phys. Chem. 99 (1995) 9822.
[18] C. Anderson, A.J. Bard, J. Phys. Chem. 101 (1997) 2611.
[19] Y. Xu, C.H. Langford, J. Phys. Chem. 101 (1997) 3115.
[20] H.-P. Lin, S. Cheng, C.-Y. Mou, Microporous Mater. 10 (1997) 111.
[21] A.L. Linsebigler, G. Lu, J.T. Yates Jr., Chem. Rev. 95 (1995) 735.
[22] A. Hagfeldt, M. Gratzel, Chem. Rev. 95 (1995) 49.
[23] A. Sclafani, J.M. Hermann, J. Phys. Chem. 100 (1996) 13655.